Volume 4
Number 4
April 2025
Pages 883-1114

Digital Discovery

rsc.li/digitaldiscovery

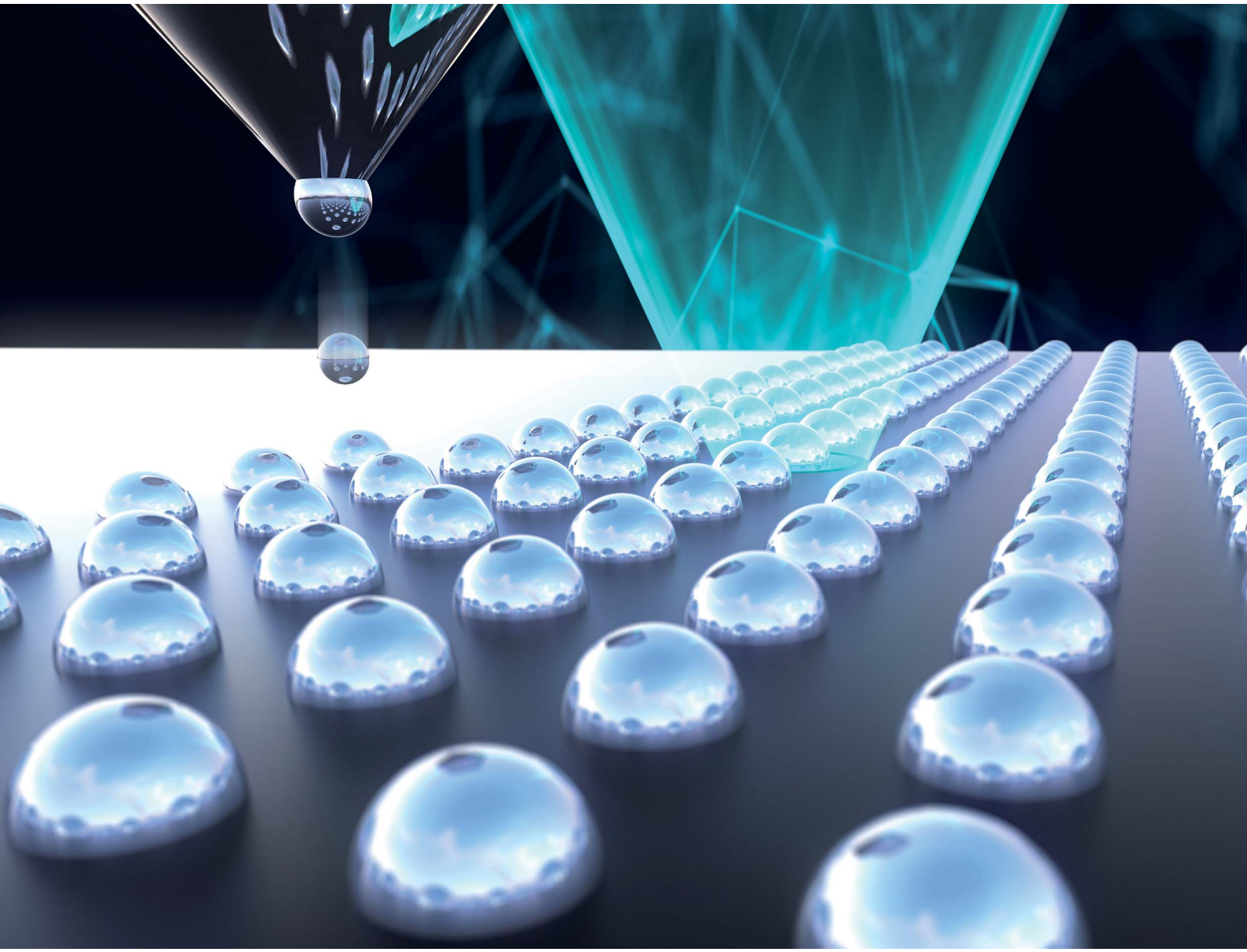

ISSN 2635-098X

ROYAL SOCIETY OF CHEMISTRY

PAPER

Alexander E. Siemenn, Tonio Buonassisi *et al.*
Archerfish: a retrofitted 3D printer for high-throughput combinatorial experimentation *via* continuous printing

Digital Discovery

ROYAL SOCIETY OF CHEMISTRY

PAPER

View Article Online
View Journal | View Issue

Cite this: *Digital Discovery*, 2025, **4**, 896

Archerfish: a retrofitted 3D printer for high-throughput combinatorial experimentation *via* continuous printing†

Alexander E. Siemenn, * Basita Das, Eunice Aissi, Fang Sheng, Lleyton Elliott, Blake Hudspeth, Marilyn Meyers, James Serdy and Tonio Buonassisi*

The maturation of 3D printing technology has enabled low-cost, rapid prototyping capabilities for mainstreaming accelerated product design. The materials research community has recognized this need, but no universally accepted rapid prototyping technique currently exists for material design. Toward this end, we develop Archerfish, a 3D printer retrofitted to dispense liquid with *in situ* mixing capabilities for performing high-throughput combinatorial printing (HTCP) of material compositions. Using this HTCP design, we demonstrate continuous printing throughputs of up to 250 unique compositions per minute, 100× faster than similar tools such as Opentrons that utilize stepwise printing with *ex situ* mixing. We validate the formation of these combinatorial "prototype" material gradients using hyperspectral image analysis and energy-dispersive X-ray spectroscopy. Furthermore, we describe hardware challenges to realizing reproducible, accurate, and precise composition gradients with continuous printing, including those related to precursor dispensing, mixing, and deposition. Despite these limitations, the continuous printing and low-cost design of Archerfish demonstrate promising accelerated materials screening results across a range of materials systems from nanoparticles to perovskites.

Received 5th August 2024
Accepted 24th January 2025

DOI: 10.1039/d4dd00249k

rsc.li/digitaldiscovery

1 Introduction

Innovation of advanced materials is key for the development of next-gen technologies. Progression of technologies such as renewable energy, efficient microchips, strong and lightweight composites, flexible electronics, and non-flammable batteries hinges on the innovation of new, advanced materials.[1–3] Historically, scientists have innovated advanced materials by cross-referencing existing literature and then modifying material recipes through domain expertise. In 1998, Rao[4] published a study documenting their successes in the discovery of novel high-performance materials through this manual, domain expertise-driven experimental procedure across a range of systems including transition metal oxides, superconducting alloys, porous solids, and nanomaterials. However, by relying primarily on domain expertise to drive materials innovation, our exploration process is limited to the bounds of human knowledge. Instead, a structured approach of exploring the complex space of material composition, crystallinity, processing conditions, and performance becomes necessary to expand the materials innovation procedure beyond the boundaries of human expertise. The concept of a multi-stage materials workflow introduced by Hanak[5] in 1970 helps develop a backbone for what this structured materials innovation procedure could look like. This structured procedure consists of the following steps: (1) synthesize many material compounds, (2) perform rapid, non-destructive chemical characterization on the compounds, (3) analyze the compound properties, and (4) acquire and process the collected chemical and property data. Today, scientists across various domains have adapted this workflow using robotics and machine learning to innovate on advanced materials.[6–9]

Many of these advancements in accelerating the materials innovation pipeline can be attributed to the recent rise in high-throughput combinatorial printing (HTCP) methods. These HTCP methods enable both the automated and fast deposition of material compounds and have shown promise across several material domains, including lithium-ion batteries,[10,11] aerosolized nanoparticles,[12] carbon nanotube composites,[13] and photovoltaic semiconductors.[14] However, much of this HTCP hardware is often cost-prohibitive for researchers, costing tens to hundreds of thousands of U.S. dollars.[8,15] Hence, there is a need for the development of low-cost HTCP methods to alleviate these cost barriers.[16] Therefore, with current manufacturing and economic advancements in precision technologies such as 3D printing,[17] some HTCP tools can be re-engineered using these low-cost technologies, in turn, increasing the accessibility to HTCP methods for materials experimentation applications.

Department of Mechanical Engineering, Massachusetts Institute of Technology, Cambridge, MA 02139, USA. E-mail: asiemenn@mit.edu; buonassisi@mit.edu

† Electronic supplementary information (ESI) available. See DOI: https://doi.org/10.1039/d4dd00249k

In this paper, we present the design of Archerfish, an open-hardware HTCP built by retrofitting low-cost 3D printer technology with rapid *in situ* fluid mixing capabilities to perform continuous printing of material compositions. These materials are treated as "rapid prototypes" such that they are created rapidly and certain have properties that transfer between scales but the materials themselves are of lower fidelity and quality than the final product. Hence, the materials synthesized by Archerfish are meant to provide high-throughput experimental input for the screening of candidate materials – these prototypes do not supplement the need to produce the final candidate materials themselves.

The name Archerfish derives from the tropical fish *Toxotes jaculatrix*, otherwise known as the archer fish for its utilization of rapidly jetting water droplets from its mouth water to strike prey from trees and branches into the water.[18] Our Archerfish tool utilizes similar droplet jetting methods but to rapidly deposit arrays of material compounds onto a substrate, rather than to strike prey, where each droplet consists of a unique material composition. Fig. 1 illustrates the design and continuous printing procedure of the Archerfish HTCP system. The ultimate design objective of Archerfish is to support general and high-throughput experimentation of materials at the bench-top scale. Archerfish has been custom-built to democratize the HTCP process through the assembly of low-cost additive manufacturing technologies, such as motion control systems, microcontrollers, and precision stepper motors. Archerfish leverages these precision motor control advancements of 3D printer technology by retrofitting the printer motion axis with a combinatorial *in situ* fluid mixing print head and multi-syringe pump assembly, controlled by a microcontroller. Through the implementation of this simple yet robust hardware architecture, we demonstrate the deposition of up to 250 unique deposited compositions per minute, across three different material systems: (1) colored dyes, (2) metal nanoparticles, and (3) perovskite semiconductors. Further information on the build instructions, unit tests, bill of materials, and design alternatives can be found in the ESI† and on GitHub: **https://github.com/PV-Lab/Archerfish**.

2 Archerfish design objectives

Archerfish was developed to democratize and simplify the hardware used for high-throughput and low-volume materials experimentation across various material domains. Since its conception, Archerfish[19] has been used to perform structured materials exploration experiments, including the rapid optimization of droplet morphology using machine learning[20] and the rapid synthesis of semiconductors for automated characterization of band gap and stability.[21] Building from these successful demonstrations of Archerfish as a tool for materials experimentation, in this paper, we aim to share its design as open-hardware for the community to use and modify for their own experimental applications. The design of Archerfish is built upon the following objectives:

2.1 Maximize throughput

We design Archerfish to maximize the number of characterizable material samples generated per unit time. Maximizing sample generation enables researchers to experimentally screen through vast material state spaces quickly to identify regions of high-performing materials. This high-throughput sample generation is also generalizable to allow interchangeability between material systems, substrates, and printing form factors to maximize utility across diverse use cases. Archerfish is designed to achieve a target throughput of 250 unique samples per minute and is demonstrated to accurately generate samples

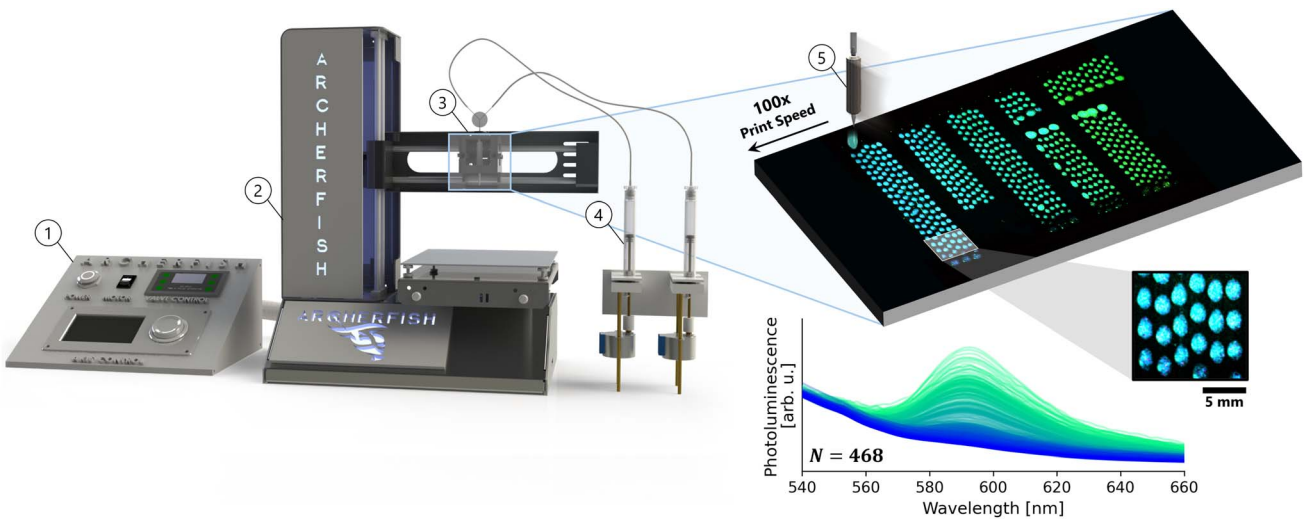

Fig. 1 Archerfish, a retrofitted 3D printer for general high-throughput combinatorial materials experimentation. (1) Control panel fitted with a pulse width modulator and microcontroller, (2) Base 3D printer (Monoprice Select Mini V2), (3) combinatorial *in situ* mixing junction and nozzle, (4) positive displacement syringe pump assembly, and (5) continuous printing speeds up combinatorial materials deposition by 100×. A gradient of $N = 468$ aqueous photoluminescent pigments is rapidly printed with Archerfish, each droplet regarded as its own unique material experiment with distinct photoluminescent spectral peak intensities.

across various material systems from colored dyes to metal nanoparticles to hybrid perovskite semiconductors while using different substrates and sample form factors.

2.2 Minimize cost

We design Archerfish to drive down the total cost of ownership (TCO) for combinatorial experimental systems:[22]

$$\mathrm{TCO} = I + N \times S, \quad (1)$$

where I is initial equipment cost, N is the number of samples created, and S is the cost per sample. Depreciation is neglected. We target minimization of the TCO for Archerfish through two design principles: (1) retrofit engineering and (2) miniaturization. Through retrofitting low-cost existing technologies, such as 3D printers, are leveraged to be built upon rather than designed from scratch, driving down initial costs, I. Furthermore, through miniaturization, the size of each sample becomes smaller, decreasing the cost per sample, S, in turn, enabling the number of samples to increase, N. Thus, it becomes economically feasible to generate thousands of individual samples. Archerfish is designed to achieve equipment costs of $I \approx 500$ USD per unit (Table S-1†) with miniaturized samples expending less than 1 μL of precursor solutions per sample.

3 Related work

Archerfish is designed to be a low-cost tool that enables small-volume, high-throughput printing of general materials *via* continuous printing paired with combinatorial *in situ* mixing. In this section, we give an overview of the prior art that we build Archerfish upon as well as the state-of-the art in the field. These topics include self-driving laboratories, low-cost high-throughput systems, and inkjet printing in materials research.

3.1 Archerfish foundations

In this section, we highlight the foundational pieces of literature upon which Archerfish was built. Firstly, before the conception of the presented version of Archerfish in this paper, several prior iterations existed with varying designs for fluid pumping, valve placement, and mixing junctions. Through trial and error and exploration of the literature, we converged on the presented design. Prior to this convergence, several systems developed for drop-on-demand (DOD) printing of materials inspired our miniaturized combinatorial printing approach. Bash *et al.*[13] use this DOD printing method with *in situ* mixing to deposit varying proportions of carbon nanotube mixtures onto a substrate for electrical characterization. Furthermore, similar DOD combinatorial printing procedures are conducted using the Opentrons overhead volumetric pipetting robot.[23,24] These DOD combinatorial printing methods often employ *ex situ* mixing, which provides precision compositional control but significantly slower throughputs. We build upon these prior methods by implementing *in situ* mixing of fluid dispensed by continuous syringe pumps. *In situ* mixing lowers the compositional control of the printing process but significantly accelerates its throughput. Furthermore, by actuating a solenoid valve on the print head, the continuous gradient-like flow of mixed fluids is broken up into miniaturized samples that are then rapidly deposited onto a substrate. Yang *et al.*[25] demonstrate accelerated throughputs in the deposition of metal oxide compounds using this inkjet printing process. Moreover, Collord *et al.*[26] implement gradient-based spray coating methods to generate over 6000 unique compositions of earth-abundant kesterite semiconductors. We have culminated these concepts of combinatorial printing by Bash *et al.*,[13] high-throughput materials inkjetting by Yang *et al.*,[25] and gradient methods to generate massive numbers of unique compositions by Collord *et al.*[26] to conceive the Archerfish HTCP tool.

3.2 Material combinatorics

Since the inception of the structured multi-stage materials research workflow proposed by Hanak in 1970,[5] similar workflows have been implemented to perform structured, combinatorial experimentation across various deposition methods, such as sputtering, inkjetting, and solution synthesis,[27] and across various scientific domains, such as catalysis, electronic materials, polymers, and biomaterials.[28] Recently, many material combinatorics studies have adopted methods of automated synthesis. Automated synthesis often utilizes a structured materials workflow, enabling them to perform experimentation significantly faster than conventional.[6,9,29]

Automated synthesis methods for combinatorics can be categorized into different classes based on how the automation itself is implemented. For example, one class includes methods that automate the process of traditional synthesis, such as automated modular microfluidic platform,[30–34] automated powder dosing and sintering platform to explore novel material candidates,[35] and automated multi-step thin film processing.[6,36–38] Another class of automated synthesis methods includes those in which one or multiple robotic arms orchestrate the motion of samples between various stations.[9,35,39] Recently, a new class of automated synthesis methods for combinatorics has emerged that leverages the speed and cost advantages of sample miniaturization.[40,41] Examples include aerosol-spray-based systems using dispensing robots[8] and nanolithography growth techniques[42] to enable high-throughput synthesis and screening of vast mega libraries of materials while utilizing low volumes of precursors. However, implementation of such robotic platforms often requires large capital investments, available to few labs or institutions. Archerfish fills this gap by offering a low-cost, sample miniaturization tool for high-throughput materials combinatorics.

3.3 Low-cost, high-throughput systems

To increase the accessibility of fast and automated materials research tools, researchers have been building low-cost devices in-house. Lo *et al.*[16] details an array of these low-cost solutions for automated research in a comprehensive review article. Researchers have been home-building these low-cost and high-throughput systems through the integration of sensor systems,

peristaltic pump liquid handling, and python-based system control.[43–45] Another level for these low-cost automated tools includes the integration of motion control systems for array-like dispensing. Xie *et al.*[46] develop a robotic platform that utilizes a 3-dimensional motion gantry system with a stepper motor syringe pump system to synthesize metal–organic materials. Archerfish embodies a similar design to that developed by Xie *et al.*[46] but also implements a material jetting technique to further boost throughputs while maintaining miniaturized samples.

3.4 Inkjet printing in materials research

Inkjet printing has emerged as the low-cost direct deposition manufacturing technique for printing a diverse array of materials.[47] The conceptual simplicity, environmental friendliness, non-contact deposition onto a substrate, and material compatibility have propelled the development of such inkjet printing methods across fields.[48] As a result, numerous successful implementations of material synthesis and deposition using inkjet printing have been demonstrated in application areas such as solar fuel cells,[49] perovskite solar cells,[50–52] oxide materials,[53] quantum dots,[54] nanoparticles,[55] cuprate superconductors,[56] and biocompatible and electroactive polymers.[57] In addition to these materials-focused applications of inkjet printing, similar methods have been applied in biological engineering for DNA synthesis[48] and drug discovery.[58]

Inkjet printing for materials applications provides both cost and time savings through the miniaturization of experiments.[59,60] Miniaturized experiments are low-volume and small, which saves on the cost of precursors but also enables many more discrete compositions to be synthesized per unit area. However, the speed of inkjet printing is often limited by the speed of ink formulation due to conventional systems not mixing inks *in situ*.[8] Archerfish overcomes this limitation by combining a solenoid valve print head for diverse ink handling[47] with an upstream continuous fluid dispensing system. By leveraging both the principles of sample miniaturization and *in situ* mixing, Archerfish is capable of performing continuous combinatorial material printing at a rate of up to 250 unique compositions per minute.

4 Continuous fluids dispensing

Archerfish continuously dispenses precursor fluids from two syringe pumps at variable rates to deposit gradients of material compounds as individual droplets. Fig. 2 illustrates the construction of the syringe pump assembly that drives the continuous dispensing. Unique precursor solutions are stored within the holding volume of the syringes, for example, $FAPbI_3$ (formamidnium lead iodide) and $MAPbI_3$ (methylammonium lead iodide), which are two different liquid formulations of hybrid organic–inorganic perovskite semiconductors.[21] These precursors are differentially pumped from the syringe holding volumes through a positive displacement pressure generated by the syringe plunger. Varying the angular velocities, ω, of the stepper motors drives a linear motion, v, of the plunger within each syringe:

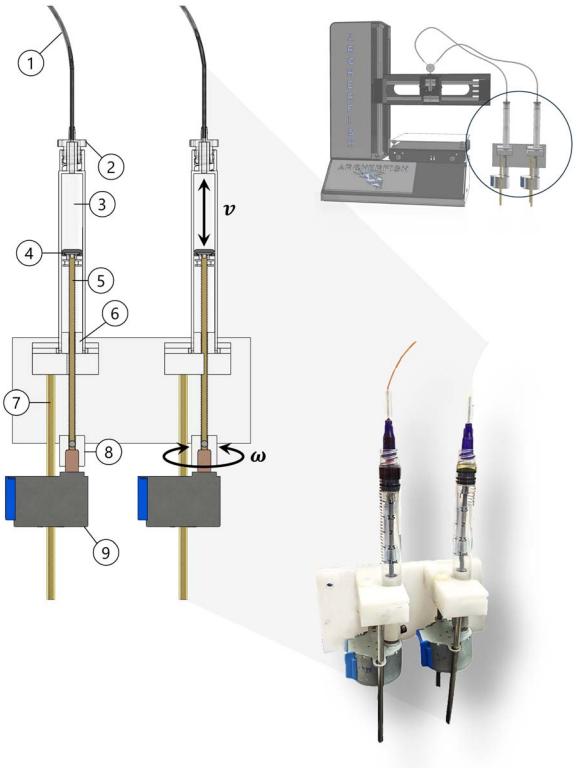

Fig. 2 Syringe pump assembly. The syringe pumps drive differential dispensing of two precursor solutions by converting the angular velocity of the stepper motors into linear velocity of the syringe plungers. (1) Outlet pipe of the syringe (1 mm ID × 2 mm OD, polytetrafluoroethylene (PTFE) tubing), (2) barbed luer lock (1.5 mm, polypropylene (PP)), (3) syringe holding volume for precursor solutions (3 mL with luer lock connection, PP), (4) syringe plunger cap (silicone), (5) threaded plunger shaft (#4–40 threads × 75 mm length, 18–8 stainless steel), (6) plunger shaft coupling to convert angular to linear velocity (#4–40 threads, polyoxymethylene (POM)), (7) stepper motor rails (3 mm diameter × 90 mm length, aluminum), (8) motor shaft coupling with lead screw (POM), and (9) stepper motors (28BYJ-48 with ULN2003 motor drivers) controlled *via* microcontroller (Arudino Mega).

$$v_{in} = P \times \omega_{in}, \tag{2}$$

where v_{in} is the resultant linear velocity of the syringe plunger, P is the pitch of the threads on the plunger shaft, and ω_{in} is the input angular velocity of the motor. Conservation of the mass flow rate within the system determines the precursor velocity at the outlet of the syringe for a given outlet cross-sectional area:[61]

$$v_{out} = \frac{v_{in} A_{in}}{A_{out}}, \tag{3}$$

where v_{out} is the outlet velocity, A_{in} is the cross-sectional area of the syringe holding volume, and A_{out} is the cross-sectional area of the outlet pipe.

The continuous dispensing of precursors forms a gradient of materials, broken up into discrete droplets that are then annealed to evaporate the solvent. For the previous example case of depositing perovskite semiconductors, the two precursor solutions $FAPbI_3$ and $MAPbI_3$ will combine to form

a continuous gradient of mixed cation compounds, $FA_{1-x}MA_x$-PbI_3, where x is the proportion of MA such that both MA and FA proportions sum to 1. In the following sections, we describe how this gradient is deposited along a tool path as either a continuous line segment or as discrete droplets, with each droplet consisting of a unique composition. To achieve accurate combinatorial ratios of precursors, the gradient must be tuned by modifying microcontroller parameters based on v_{out} and the path length of the outlet pipe.

5 Combinatorial fluids mixing

Archerfish performs *in situ* mixing of dispensed material precursor fluids to deposit homogeneously mixed compounds along a tool path. As the precursors flow from the syringe pump holding volume ((3) in Fig. 2) to the micro-nozzle exit ((7) in Fig. 3), they combine from two independent flows to a single flow through a Y-junction ((3) in Fig. 3). The single flow then passes through a solenoid valve ((5) in Fig. 3), which actuates at a frequency and duty cycle specified by a pulse width modulator (PWM) in the controller to break up the flow. The broken-up flow gets focused through a micro-nozzle and ejected onto a substrate placed on top of the build plate of the 3D printer. The PWM frequency and tool path speed determine whether continuous gradients or discrete droplets of material compounds are deposited. These actuation and focusing properties of the solenoid valve and nozzle are the key determiners of mixing quality in Archerfish. There is approximately 50 μL of internal volume within the plumbing of Archerfish, including the Y-junction and solenoid, and the volume of each deposited droplet varies between 1–10 μL depending on the printing parameters. Hence, there is a response latency between the input to a syringe pump and the output composition, which is calibrated to ensure that gradient mixing and deposition begin at the desired point after purging. It should be noted that droplet mixing quality is also dependent on fluid viscosity, the tendency for phase separation, and micro-nozzle geometry.

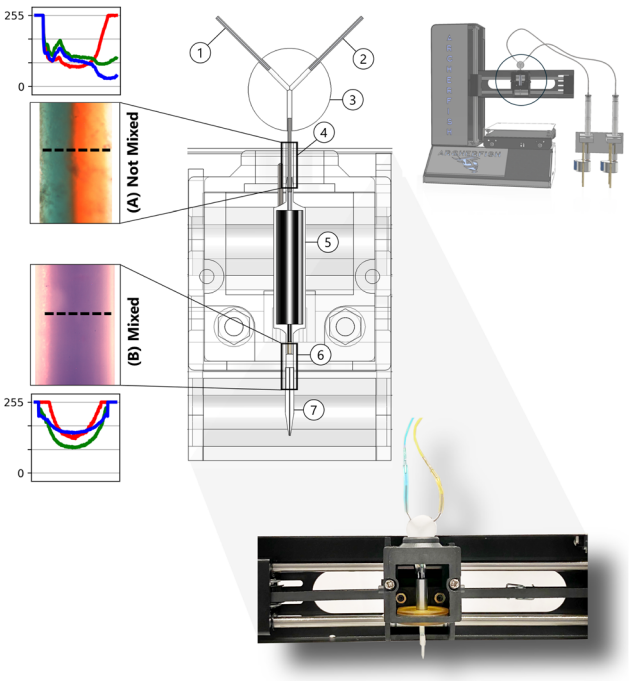

Fig. 3 Pulsation-induced *in situ* mixing for combinatorial fluids printing image by optical microscopy in transmission mode. (A) Before the solenoid valve, blue and red colored dye flows combine into a single flow. The fluids do not mix because they are in the laminar flow regime. The discontinuity of RGB color traces quantifies the absence of mixing along the diameter of the pipe (black dashed line). (B) The combined blue and red flow after passing through the actuating solenoid valve. The RGB traces smooth and blend together to become purple, demonstrating the effect of pulsation-induced mixing by the solenoid valve. (1) Left precursor inlet (0.559 mm ID × 0.635 mm OD, 304 stainless steel), (2) right precursor inlet, (3) flow-combining Y-junction (polyoxymethylene (POM)), (4) junction-to-solenoid coupling (silicone rubber), (5) actuating solenoid valve (6 mm INKA2424212H VHS Series P–P, The Lee Company) controlled by a PWM (ZK-PP2K), (6) solenoid-to-nozzle coupling (silicone), (7) flow-focusing micro-nozzle outlet (300 μm diameter, 1551-120-437P 200(10-11D-20), Small Precision Tools).

5.1 Pulsation-induced mixing

Fig. 3 illustrates the print head assembly of Archerfish retrofitted with a Y-junction to combine flows, a solenoid valve to pulse and mix the flow, and a micro-nozzle to focus the flow and form discrete droplets. Pulsation-induced mixing occurs within the control volume of the solenoid valve. External pulsations or perturbations within a laminar flow are necessary to induce mixing without the use of static mixing obstacles.[62,63] The Reynolds number measures the ratio of inertial to viscous forces within a flow, which determines whether the flow regime is laminar or turbulent:[64]

$$\mathrm{Re} = \frac{\rho v D}{\mu}, \tag{4}$$

where Re is Reynolds number, ρ is fluid density, v is fluid velocity, D is the pipe diameter, and μ is the fluid viscosity. A laminar flow regime occurs below the threshold of Re = 2100.[65] A turbulent regime occurs above this Re threshold. In Fig. 3A, the laminar nature of this flow is observed. Even though the two independent fluid paths combine into a single flow after the Y-junction, the strength of the viscous forces is strong enough to inhibit the flows from mixing. A discontinuity in the RGB traces of fluid color across the pipe diameter demonstrates the absence of mixing. Thus, actuation of the solenoid creates pulses within the originally laminar flow, generating turbulence and, in turn, mixing the streams.[63] Fig. 3B shows the flow after passing through the solenoid valve. The smooth RGB traces of fluid color across the pipe diameter indicate that mixing is achieved. Further mixing occurs at the exit point of the micro-nozzle through vortical motion induced by the nozzle's flow-focusing geometry.[66]

5.2 Vortex-induced mixing

The micro-nozzle exit of the Archerfish print head is conical to constrict the fluid flow, enabling rapid jetting and break-up of the mixed fluid flows into discrete droplets with the assistance

of the solenoid valve actuation. When the solenoid gate closes during actuation, fluid is rapidly displaced and jetted out from the control volume. When the solenoid gate opens, fluid flows through the control volume and surface tension forms a droplet attached to the nozzle tip.[67,68] Due to the spherical shape of the droplet in this formation stage, a circulation zone forms and generates a vortex flow.[66] This circulating vortex flow during the formation stage of a droplet is shown in Fig. 4A. Vortices within a droplet further drive the mixing of solutions to produce a homogeneously-mixed product.[69,70] Through this flow pulsing of the solenoid valve and the flow focusing of the micro-nozzle, precursor solutions are mixed and jetted onto a substrate as unique material compositions.

Fig. 4B demonstrates the mixing capabilities of Archerfish using 100 nm diameter silicon (Si) and titanium (Ti) nanoparticle suspensions, imaged by scanning electron microscopy (SEM) and energy-dispersive X-ray spectroscopy (EDX). Si and Ti nanoparticle suspensions are prepared at 5 wt%, respectively, in deionized water and ultrasonicated to form suspensions. To unit test the compositional mixing capabilities of Archerfish, these nanoparticle suspensions are loaded into the syringe pumps and dispensed by driving both pumps at equal flow rates to form droplets of equal parts silicon to titanium nanoparticles. Uniform deposition of the Si–Ti mixtures can be seen in both the SEM and EDX images after evaporating the water from the deposited droplet. An even distribution of Si nanoparticles (light regions of SEM and pink regions of EDX) and Ti nanoparticles (dark regions of SEM and blue regions of EDX) can be seen throughout the imaging field, demonstrating the mixing methods sufficiently combining and mixing the individual nanoparticle precursors. Within the EDX image field, the atomic percent contributions of each element are quantified to be 51.2 at% and 48.8 at% for Si and Ti, respectively, achieving the expected 50.0 at.%-to-50.0 at% ratio within 1.2 at% error.

6 High-throughput materials printing

6.1 Benchmarking

To benchmark the continuous printing performance of Archerfish, we compare its output with an Opentrons volumetric pipetting robot commonly used in automated experimental research.[23,24] Opentrons utilizes stepwise printing with

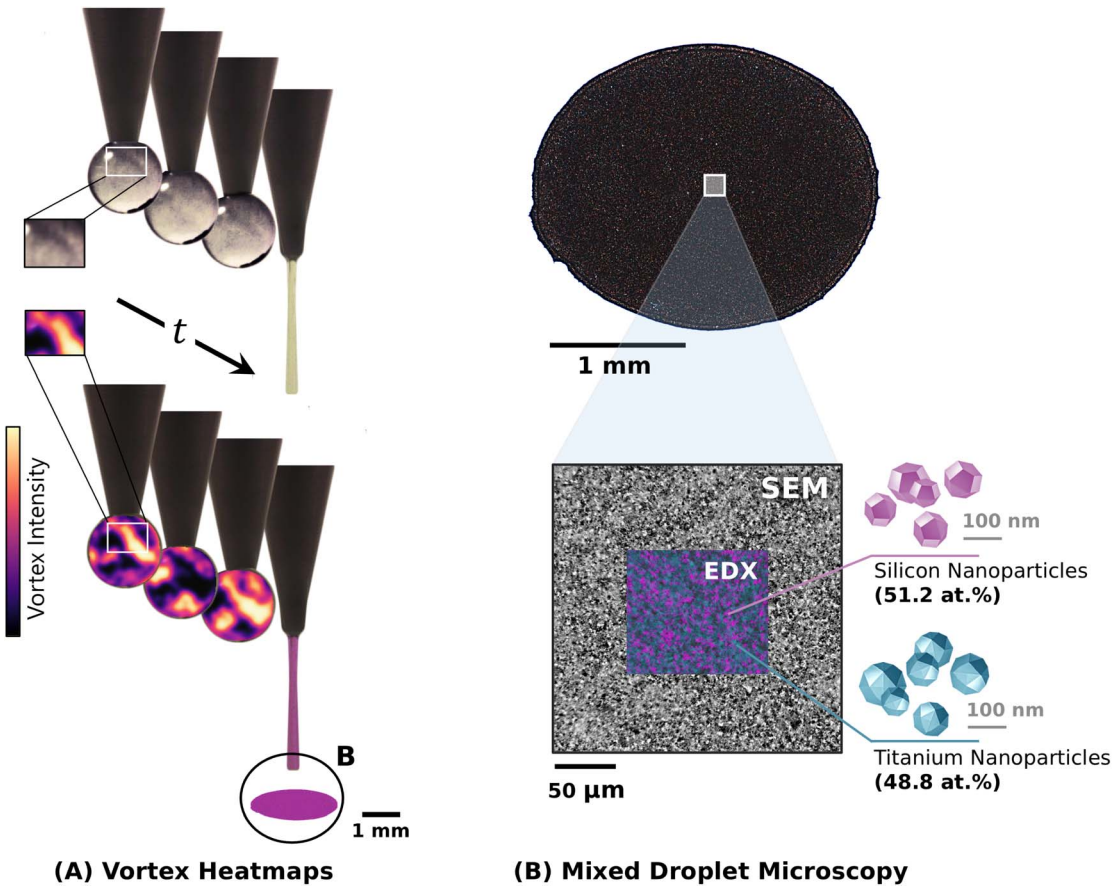

Fig. 4 Microscopy of a mixed droplet printed by Archerfish. (A) Vortex-induced mixing within a droplet forming at the tip of the micro-nozzle. (Top) Four frames of an RGB video taken over a time step, $t = 0.28$ seconds, showing vortex circulation within a formed droplet and jetting. (Bottom) Heat map overlays of the vortex flow obtained by computing the pixel-wise intensity differences along the green channel of adjacent video frames under fixed lighting conditions. Bright regions of the heat map indicate high vortex motion over time. (B) (Top) Optical microscope image of a full Archerfish droplet printed using silicon (visualized as pink) and titanium nanoparticles (visualized as blue). (Bottom) Scanning electron microscopy (SEM) image of the deposited nanoparticles within a region of the deposited droplet. A region of the SEM image is measured using energy-dispersive X-ray spectroscopy (EDX) to visualize and determine the atomic percent contribution of each element within the region.

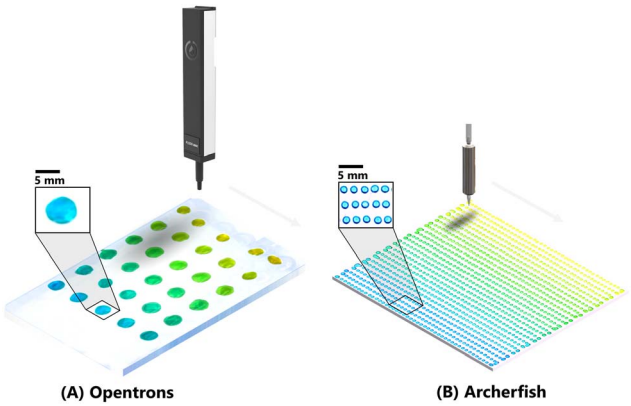

Fig. 5 Combinatorial printing throughput comparison between Opentrons and Archerfish. (A) Opentrons printing of colored dyes at a rate of 2.5 unique compositions per minute with *ex situ* mixing and stepwise printing. (B) Archerfish printing of colored dyes at a rate of 250 unique compositions per minute with *in situ* mixing and continuous printing.

ex situ mixing to perform combinatorial drop-casting. Materials are printed in a stepwise fashion by mixing each set of precursor solutions, which in this demonstration are blue and yellow dyes, *ex situ* in an auxiliary mixing vessel such as a 96-well plate. By varying the proportions of each precursor fluid dispensed into each well of the auxiliary vessel, a gradient of materials can be mixed through orbital shaking or aspiration. Then, the mixed fluid is aspirated from the vessel and deposited *via* drop-casting with certain volumes onto a substrate. This *ex situ* mixing process is highly accurate because the exact proportions of each precursor can be precisely dispensed and mixed. In Fig. 5A, we illustrate Opentrons drop-casting a 5 × 6 gradient array onto a glass substrate. Although this *ex situ* mixing procedure is highly accurate, it is slow – here, a throughput of only 2.5 unique compositions per minute is achieved.

Conversely, in Fig. 5B, we illustrate Archerfish continuously printing with *in situ* mixing, to rapidly print a 45 × 26 gradient array onto a polyester substrate. With this continuous dispensing of precursors into an *in situ* mixing junction, mixed through solenoid perturbation and vortices, a throughput of up to 250 unique compositions per minute is achieved, 100× faster than Opentrons stepwise printing with *ex situ* mixing. Although this *in situ* mixing process is fast, results are not as precise as *ex situ* mixing due to mixing quality and gradient formation becoming a function of fluid viscosity, plumbing line length and diameter, and flow velocity. In the latter sections, we quantify this error in compositional control and accuracy of *in situ* mixing using energy-dispersive X-ray spectroscopy. However, with proper calibration, a diverse range of material systems can be successfully printed at high-throughputs using Archerfish.

6.2 Experiments

The proposed Archerfish architecture is a versatile platform with interchangeable material form factors, substrates, and printable compounds, enabling general HTCP materials experimentation. We demonstrate this generalizable nature of Archerfish by continuously printing miniaturized material samples while varying all three of these features. *Form factors*: (1) hundreds of small droplets closely packed, (2) continuous line segments, and (3) tens of larger droplets loosely packed. *Substrates*: (1) polyester sheet with a hydrophobic coating, (2) sanded copper plate with 3 mm diameter hemispherical wells, (3) glass slide. *Material compounds*: (1) colored dyes, (2) metal nanoparticle alloys, (3) hybrid inorganic–organic perovskite semiconductors. Fig. 6 illustrates the experimental results from these three unique printing procedures. The formation of a material gradient is illustrated using Hyperspectral imaging data from each substrate. Hyperspectral imaging validates the formation of compositional gradients across the three material systems by capturing the unique compositional signature within each material's reflectance spectrum. Here, we utilize a Resonon Pika L Hyperspectral camera with a white LED line light to capture spectral reflectance intensity information along 300 wavelength channels per pixel. Then, across all the pixels for each droplet, the average spectrum is calculated and visualized, pairing its position on the substrate to a corresponding color bar color.

Fig. 6A demonstrates the close packing of many small droplets of blue-to-yellow colored dyes onto a polyester substrate. The printing throughput of Archerfish for this experiment is 250 unique compositions per minute. The continuous printing procedure trades off the ability to print singular compositions with the ability to print continuous gradients of compositions quickly. In Fig. 6(A3) we use Hyperspectral imaging to analyze the unique spectral signatures of each deposited composition and demonstrate an accurate spectral shift in composition corresponding to the programmed gradient printed from blue dye to yellow dye. As the proportion of yellow dye increases within each droplet, the blue spectral peak (400–500 nm) diminishes while the yellow spectral peak (500–600 nm) rises, validating the formation of the blue-to-yellow colored dye gradient.

Fig. 6B demonstrates the formation of line segments of titanium–silicon metal nanoparticle alloys onto a sanded copper substrate. For this experiment, 20 layers of identical gradients are printed on top of each other to form thick line segments. Prior to printing, 81 hemispherical wells are drilled into the substrate to serve as the measurement points for hyperspectral reflectance. The printing throughput of this experiment is 4 unique line segments per minute. Although the formation of a material gradient is not visually perceivable, it is detected through hyperspectral imaging. Here, we see as the proportion of silicon nanoparticles rises relative to titanium, the reflectance spectrum biases downward. The signal of this trend is noisier due to many layers of nanoparticles being imperfectly deposited on top of each other, blurring the hyperspectral signal.

Fig. 6C demonstrates the loose packing of large droplets of $FAPbI_3$–$MAPbI_3$ (formamidnium lead iodide–methylammonium lead iodide) organic perovskite semiconductors onto a glass substrate. The printing throughput of this experiment is 250 unique compositions per minute. Similar to the

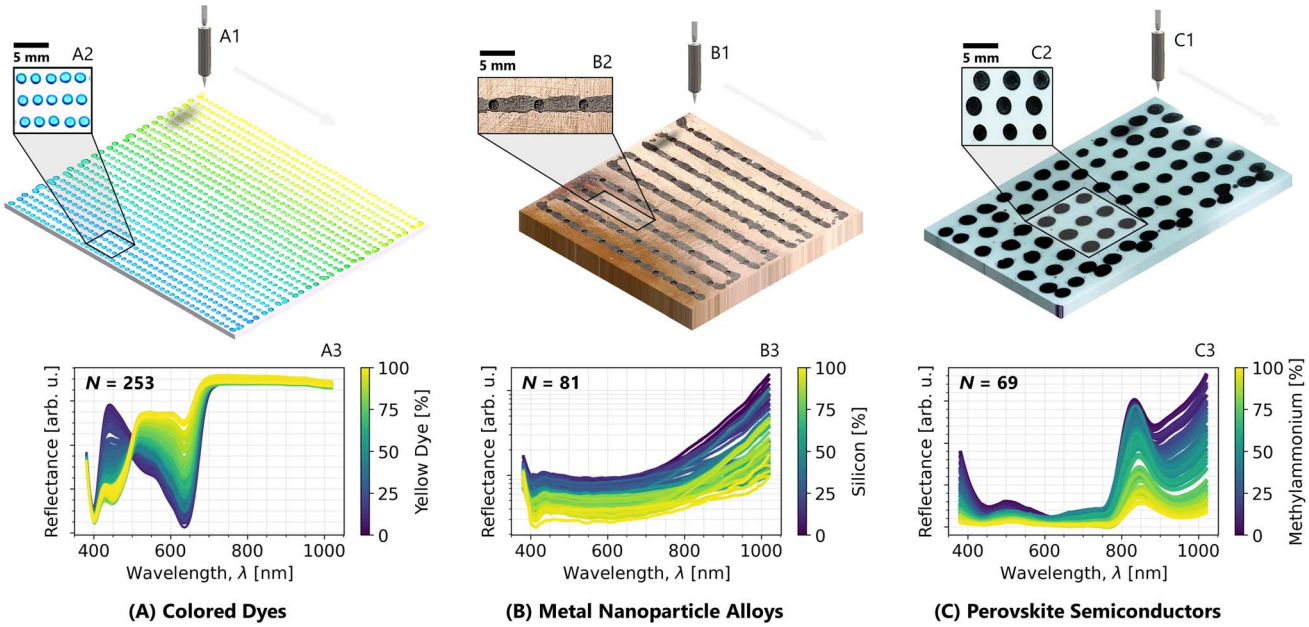

Fig. 6 General high-throughput combinatorial printing use-cases of Archerfish. Demonstrated deposition and optical characterization of (A) blue-to-yellow colored dye, (B) titanium–silicon metal nanoparticle alloys, and (C) formamidnium lead iodide–methylammonium lead iodide ($FAPbI_3$–$MAPbI_3$) hybrid organic–inorganic perovskite semiconductors. The Archerfish print head follows a tool path to print (A1) a gradient of 253 closely packed droplets onto a hydrophobic coated polyester sheet (100 mm × 100 mm, PP2500, 3M), (B1) 20 layers of continuous gradient line segments lines onto a sanded copper plate (80 mm × 80 mm) with 3 mm diameter hemispherical wells, and (C1) a gradient of 69 loosely packed, large droplets onto a glass slide (50 mm × 75 mm). Magnified views of the (A2) dye droplets, (B2) metal alloys, and (C2) perovskite semiconductors. Hyperspectral reflectances of all printed samples for the (A3) dye droplets, (B3) metal alloys, and (C3) perovskite semiconductors.

metal nanoparticles experiment, the formation of a gradient is not perceptible to the eye because most of the $FAPbI_3$–$MAPbI_3$ spectral shift occurs in the infrared region, detectable by hyperspectral imaging. As the proportion of methylammonium in the composition increases, the infrared peak shifts from 825 nm to 850 nm while the peak intensity decreases. These hyperspectral reflectance peaks are related to the semiconductor material property of band gap, which we further explore in a separate paper.[21]

Here, we demonstrate the successful printing of three different material system gradients across three different form factors at a rate of up to 100× faster than similar hardware by utilizing continuous printing and *in situ* mixing of the Archerfish design. Furthermore, we validate the formation of compositional gradients by analyzing the unique spectral signature of each material with hyperspectral imaging and analysis.

7 Documentation

The Archerfish system costs approximately 500 USD to build (Table 1), approximately 30× lower than the price of common commercial pipetting systems. A general bill of materials is provided in Table S-1† while a complete bill of materials, operating code repository, and design assembly of Archerfish are available on GitHub: **https://github.com/PV-Lab/Archerfish**. Note that many components were made in-house and require some machining and basic soldering. The reader is instructed to use the detailed design assembly provided in the GitHub repository and in the ESI† for guidance on the manufacturing and assembly of these components.

Table 1 Bill of materials to construct an Archerfish unit

Description	Cost (USD)
Solenoid valve	183.58
3D printer	175.99
Micro-nozzle	50.00
Arduino mega	48.90
Fittings, tubing, and pumps	23.39
PWM driver	10.57
Buttons and switches	8.82
Motors	5.90
Total	**507.15**

8 Limitations and solutions for overcoming them

The architecture presented for high-throughput combinatorial printing with Archerfish is promising and has been used to print gradients of several different material systems.[20,21] However, with its current design, Archerfish has limitations that require additional calibration time to address that can otherwise result in poor reliability and reproducibility of samples. These limitations can be categorized into three main buckets: compositional control, droplet generation, and environmental

and crystallization control. Each category has unique limitation considerations for the current tool but also invites opportunities for growth and design.

8.1 Lack of compositional control

Compositional control refers to the ability to set and determine the compositions of individual droplets. With Archerfish's current architecture, it is challenging to set a specific composition for each droplet or determine a droplet's exact composition without additional measurements, such as EDX. Compositional control can be further limited by various factors but major contributors such as pressure build-ups and fluid reservoirs have been identified and are further discussed here. However, with careful calibration of the printing parameters, it is possible to control the composition of gradient printing with known endpoints that are pre-loaded as precursors in the syringes.

8.1.1 Limitations. The lack of compositional control reduces the reliability of Archerfish and makes it more difficult for researchers to use the system. For example, it took three researchers two days to find the right parameters to create an end-to-end gradient for the $FAPbI_3$–$MAPbI_3$ perovskite series due to the complex relationship between the droplet wetting properties, reservoirs, compliant regions, and standing waves within the fluid lines. Fig. 7 illustrates the EDX-measured elemental traces of an 80-droplet $Cs_3Bi_2I_9$–$Cs_3Bi_2Br_9$ (cesium bismuth iodide–cesium bismuth bromide) perovskite series printed with Archerfish that did not have its printing parameters properly tuned. This improper tuning resulted in approximately only 80% of the entire gradient being printed, stopping before reaching the $Cs_3Bi_2Br_9$ end point. Furthermore, pressure built-ups in areas of compliance within the fluid lines create non-linearities in flow rates. For example, the syringes use a silicone rubber plunger and as a result, fluid is not always dispensed when the motors push the plunger, instead, the plunger compresses to accommodate the resulting pressure from the positive displacement. Discontinuities in expected flow rates are also linked to the pressure build-up in the compliant plunger or fluid lines. Another main hindrance to compositional control is the presence of fluid reservoirs that result in hard-to-predict mixing behavior, which ultimately average out to produce a gradient, but do not seem to be linear at each time step. Reservoirs within the valve generate vortices and can result in residual contamination that complicates the transition between fluids, producing unknown compositions at the output droplet. Lastly, important questions regarding the impacts of pressure, fluid viscosity, temperature, and other parameters on fluid composition and deposition require further analysis and study.

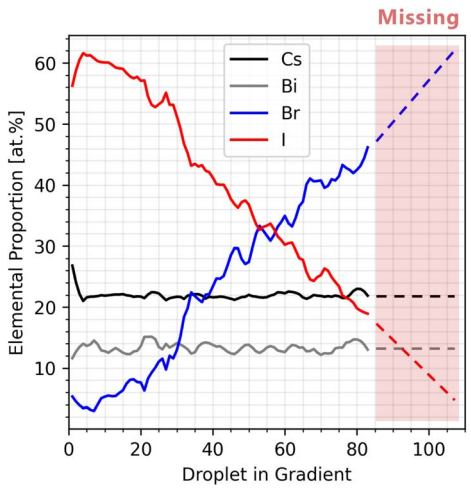

Fig. 7 Energy-dispersive X-ray spectroscopy (EDX) elemental composition traces. These elemental traces are shown for a $Cs_3Bi_2I_9$–$Cs_3Bi_2Br_9$ (cesium bismuth iodide–cesium bismuth bromide) perovskite gradient printed using Archerfish where each droplet has its EDS spectrum measured. We note the abrupt stop in the compositional shift between iodine and bromine due to improper tuning of the Archerfish print settings. Approximately 80% of the entire gradient is shown to be successfully printed here, the missing portion of the gradient is projected using dashed lines.

8.1.2 Solutions. With the correct printing parameters, it becomes possible to better control the gradient compositions of materials output by Archerfish. The length of the gradient is tuned by modifying the stepper motor ramp-up or ramp-down accelerations, $\dot{\omega}$, in the microcontroller. When changing the substrate size or the tool path speed, $\dot{\omega}$ must be modified to accommodate the full gradient. If the substrate size decreases in printable area, $\dot{\omega}$ must be increased to accommodate a shorter gradient. Conversely, if the translation speed of the print head decreases to form more closely packed droplets, $\dot{\omega}$ must be decreased to accommodate a longer gradient. The printing speed and path are tuned by modifying the G-code parameters. G-code is a set of numerical commands used to control the linear and angular positions of stepper motors within a system.[71] The G-code of Archerfish has two main tunable parameters: positional coordinates and translation speed. The generation of many closely packed droplets represents our base case for G-code parameters, which has a tool path spacing width of 3 mm along the *Y*-axis. To generate continuous line segments, the positional coordinates are further spaced along the *Y*-axis in the G-code, relative to the base case, to prevent the cohesion of independent line segments along the *Y*-axis. Furthermore, the tool path speed is decreased to promote the cohesion of individual droplets along the *X*-axis to form continuous line segments. To generate few larger, loosely packed droplets, the positional coordinates are further spaced along both the *X*- and *Y*-axes to prevent cohesion while translation speed remains the same. In general, the slower the tool path, the wider spacing required. To assist researchers in utilizing Archerfish for high-throughput materials experiments, we provide all printing parameters used for perovskite printing as open-access microcontroller code and G-code available on our GitHub repository. To solve the non-linearities due to build-up or cross-contamination, we have implemented reservoir purging processes into our open-access code. These purging processes sometimes take much longer than the prints themselves, sometimes up to a minute, and waste precursors but greatly improve the reproducibility and control of gradient compositions between runs. Further

reduction of non-linearities has been implemented by replacing deformable tubing with rigid, noncompliant tubing.

8.2 Droplet generation

Archerfish can deposit gradients of uniformly thick droplets on most prints, but this uniformity can vary based on the precursor molarity and properties of the fluid or substrate. Substrates with higher wettability often distort the droplets, limit droplet packing, and add variability to their shape. Moreover, the relationship between droplet shape and the PWM driver has not been characterized in detail, making it difficult to change the droplet generation parameters along with the gradient parameters in accordance with the substrate wettability. However, by tuning the PWM parameters, it is possible to achieve target droplet geometries, which can be maintained across prints to improve reproducibility.

8.2.1 Limitations. Archerfish droplets of inorganic composition with low molarity demonstrate coffee ring effects after annealing. Higher evaporation rates at the droplet's edge cause radial migration of the species in the fluid. This phenomenon produces a droplet with a thicker outer ring of high species concentration and a thinner inner area of low species concentration.[72] Fig. 8 illustrates these differences in species migration rates for different molarity Archerfish droplets. The thickness profile of a more uniformly thick droplet is shown in Fig. 8a, and the thickness profile of a non-uniform droplet exhibiting the coffee ring effect is shown in Fig. 8b. Furthermore, the merging of droplets, non-uniform droplet deposition, and formation of satellite droplets can result in inconsistent printing results across experiments.

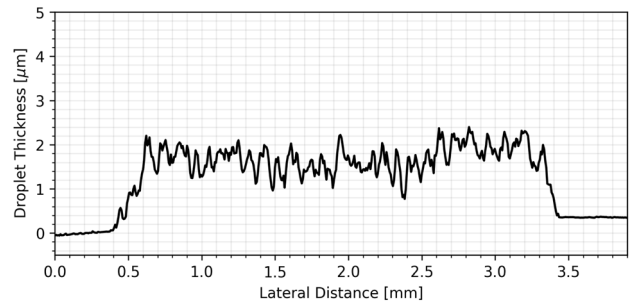

(a) $FAPbI_3$-$MAPbI_3$ Droplet Thickness Profile

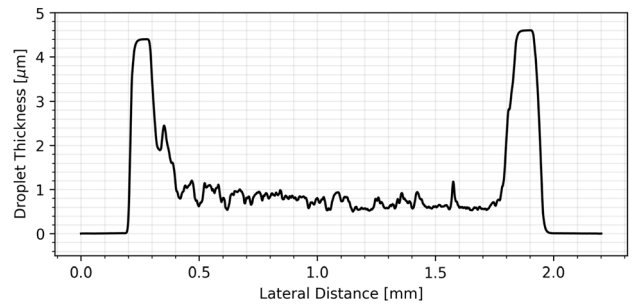

(b) $Cs_3Bi_2Br_9$-$Cs_3Sb_2I_9$ Droplet Thickness Profile

Fig. 8 Thickness profiles of Archerfish-deposited perovskite droplets obtained using surface profilometry. (a) Organic $FAPbI_3$–$MAPbI_3$ perovskite droplet with 0.6 molarity. (b) Inorganic $Cs_3Bi_2Br_9$–$Cs_3Sb_2I_9$ (cesium bismuth bromide–cesium antimony iodide) perovskite droplet with 0.1 molarity. Different molarity droplets have varying rates of evaporation between the edge and center. The high-molarity organic-cation (MA, FA) material depositions have thicker and more even profiles on average. Conversely, the low-molarity inorganic Cs material depositions are thinner and experience species migration, accumulating material around the edge to create a coffee ring effect.[72]

8.2.2 Solutions. Downstream post-processing and characterization techniques can be used to minimize the effects of this coffee ring phenomenon in most cases. Although not a function of Archerfish printing, tuning the annealing conditions for a given material system can accelerate or hinder the migration of material to alter the formation of coffee rings.[72] Furthermore, the coffee ring effect is mostly seen only on the very outer edges of a droplet, as shown in Fig. 8b, thus, by focusing characterization on only the inner region of the droplet, coffee ring effects can be avoided. To address the limitations in droplet formation and generation, the PWM parameters are carefully tuned based on the desired droplet output. The PWM has three tunable parameters: voltage, frequency, and duty cycle. Voltage determines the strength of actuation, frequency determines the periodicity of actuation, and duty cycle determines the open-to-close ratio of the solenoid gate for each period. To generate many closely packed droplets, we tune the PWM frequency to 20 Hz and 19% duty cycle. To generate continuous line segments, we maintain the 20 Hz frequency but lower the duty to 7%. Lastly, to generate few loosely packed droplets, we decrease the frequency to 5 Hz and use a moderate duty of 11%. For all deposition cases, we supply the PWM with 24 V to preserve consistent actuation force. Safety of the user should be considered when modifying PWM parameters. The PWM is responsible for actuating the flow gate. Hence, forgetting to activate the PWM or modifying the PWM parameters such that a closed gate is maintained for prolonged periods causes fluid to build up within plumbing lines. These safety concerns have been addressed in Archerfish by replacing compliant silicone tubing with rigid, non-compliant PTFE tubing to minimize regions of potential fluid build-up up in addition to only operating Archerfish within a fume hood or glovebox when working with hazardous precursor materials.

8.3 Environmental and crystallization control

Environmental and crystallization control refers to the ability to control and create uniform crystallization conditions across all droplets on an Archerfish print. Crystallization control is not necessary for all Archerfish samples, however, some material systems cannot be studied without it. Since Archerfish is designed to be a general experimental tool, no aspect of the device is devoted to post-processing any one specific material system. For example, Archerfish does not maintain a constant temperature, pressure, or humidity around samples while or after they are printed, as these conditions would vary across different material systems.

8.3.1 Limitations. This lack of environmental control presented a challenge for the synthesis of perovskite gradients, limiting our ability to study crystallization-dependent

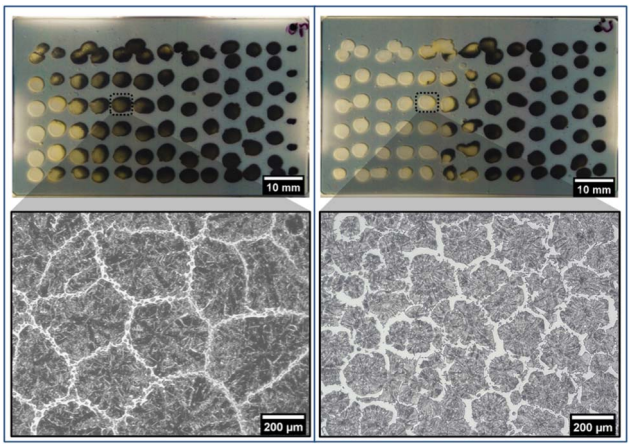

Fig. 9 Two different Archerfish prints of the same $FAPbI_3$–$MAPbI_3$ compositional gradient after annealing and controlled degradation. Yellow samples are degraded while black samples are not degraded. These two perovskite gradients exhibit different degradation patterns despite being of the same composition and degrading under the same conditions. The differences in crystallization, as shown by the SEM images, transpired from spatial non-uniformities in the annealing and deposition processes.

properties like stability. Inconsistent degradation patterns across Archerfish prints arose due to the non-uniform crystallization of droplets. Fig. 9 shows the controlled degradation of two perovskite samples of the same $FAPbI_3$–$MAPbI_3$ compositional gradient. Varying degradation patterns were observed and are believed to be due to non-uniformities hot plate temperatures during annealing as well as inconsistent temperatures, humidities, and high gaseous solvent concentrations during deposition.

8.3.2 Solutions. To overcome the coupled challenges of environmental and crystallization control, an ideal solution is to enclose Archerfish within a regulated and controllable environmental enclosure. This type of enclosure receives feedback from the internal environment to modulate temperature and the supply of dry air or inert nitrogen gas to maintain consistent humidity. Due to the engineering complexity of designing a controlled enclosure, we have found success in controlling reproducibility across experiments by simply measuring these critical variables temporally using sensors to ensure each experiment is conducted within similar environmental conditions. For example, we have set up a network of temperature, humidity, and solvent concentration sensors to log information about the current environment during printing, allowing informed identification of potential root causes of unexpected degradation or poor crystallization.

8.4 Future work

Beyond the concerns presented by a lack of compositional control, droplet generation, and environmental and crystallization control, several minor but impactful limitations warrant a mention. Many of these limitations are currently being addressed in future works.

8.4.1 Limitations. Due to the stepwise rotation of the stepper motors, the syringe pumps create oscillations in the fluid flow that do not affect the overall gradient composition but could impact the composition of individual droplets. The current wetted materials in the Archerfish plumbing lines are PTFE, silicone, and polypropylene. While PTFE is resistant to a wide range of chemicals, silicone and polypropylene are not, which limits the materials that can be studied with the current Archerfish design. Although some mixing occurs at the tip of the orifice, as shown in Fig. 4, precursor flows with higher viscosities or lower Reynolds numbers could require more folds or obstacles within the plumbing lines to promote more uniform mixing. There are further implications regarding the effects of viscosity on droplet generation, which would require significant recalibration of parameters to maintain compositional control as precursor viscosity increases. Overpressurization and back-flow in the fluid lines further limit compositional control and create leaks in the system. Moreover, manually handling and moving the printed-on substrates can agitate the droplets causing them to shift and change shape. Lastly, full integration of each Archerfish subsystem is lacking. The retrofitted 3D printer, PWM, and microcontroller are all independently controlled, with no central data center to set the parameters or make changes to the gradient parameters. This leads to variations across prints since all three subsystems are not always activated synchronously. These variations can be further exacerbated by the lack of real-time data acquisition during the printing procedure.

8.4.2 Solutions. To address some of the limitations described in this paper, further design work is needed. A new pump design could eliminate the oscillations in the fluid flow while also increasing the chemical resistance of the path of the wetted materials. Handling of precursors with different viscosities would require the implementation of more complex mixing obstacles to promote uniform mixing in addition to modifying the pump rates according to the viscosity delta between precursors to attain gradient compositional control. To further improve reliable compositional and crystallization control between experiments, Archerfish should built into an environmental enclosure for better environmental control with stations for post-processing materials. Further studies are being done to understand droplet deposition and eliminate the formation of satellite droplets. Drop casting is being explored instead of inkjet printing for more consistent and uniform droplets. Integrating all subsystems into one control center could improve synchronization for more controlled and reproducible deposition. Lastly, automation, such as the transfer of samples using robotic arms, could be utilized for sample handling to limit the adverse impact of vibrations and jerk on droplet morphology.

9 Conclusion

In this paper, we highlight the design and development of Archerfish, a retrofitted 3D printer for general high-throughput experimentation *via* continuous printing. The key design features of Archerfish include microcontroller-driven continuous dispensing of solution-based material precursors, multi-fluid mixing of laminar flows, and modular components

easily installable onto existing 3D printer technology. The culmination of these design features drives rapid and continuous combinatorial deposition of materials as discrete droplets at rates of up to 250 unique compositions per minute, an acceleration factor of 100× compared to existing methods. Leveraging these accelerated printing throughputs enables the fast screening of new candidate materials as "rapid prototypes" prior to down-selection.

We demonstrate this combinatorial continuous printing of Archerfish on three unique material systems, each with a different substrate and printed form factor. The three material systems span from colored dyes to metal nanoparticles to perovskite semiconductors. We analyze the unique spectral signature of each deposited material with hyperspectral imaging to validate the presence of continuous composition gradients for each material experiment. In each of these three materials experiments, a gradient is shown to exist across the printed materials through a gradual shift in the spectral reflectance. Furthermore, we highlight the limitations of the current Archerfish architecture for materials experimentation. However, despite these limitations and needs for design advancements, successful materials research has been conducted with Archerfish in the machine learning-guided optimization of droplet morphology[20] and exploration of semiconductor band gaps and stabilities.[21] The utilization of Archerfish as a generalizable tool for high-throughput combinatorial materials research opens the door for scientists to explore vast material spaces and rapidly test experimental hypotheses at a low cost, thereby expanding the accessibility of designing new materials across a range of applications.

Data availability

Data for this article, including EDS, hyperspectral, and profilometry data as well as the microcontroller code, comprehensive bill of materials, and complete hardware assembly file are available on GitHub at **https://github.com/PV-Lab/Archerfish**.

Author contributions

A. E. S., J. S., and T. B. conceptualized the work. A. E. S., B. D., and T. B. designed the methodology. A. E. S., B. D., E. A., L. E., B. H., M. M., and J. S. designed and built the hardware and electronics. A. E. S., E. A., and L. E. wrote the software. A. E. S., B. D., E. A., F. S., and M. M. conducted experiments. A. E. S., B. D., and E. A. wrote the manuscript. All authors reviewed and edited the manuscript. A. E. S., B. D., and T. B. provided guidance.

Conflicts of interest

There are no conflicts to declare.

Acknowledgements

The authors acknowledge Shijing Sun and Liu Zhe for their discussions and input during the early development of Archerfish. A. E. S. acknowledges Nadya Peek, Lilo Pozzo, and the other participants of the "Pathways to Open-Source Hardware for Laboratory Automation" workshop, as this paper would not exist without their fruitful discussions on open hardware. The authors acknowledge Emre Tekoglu, Armi Tiihonen, Elena Botica Artalejo, and Hamide Kavak for their assistance in preparing precursors and substrates for printing. The authors acknowledge funding support from: the Defense Advanced Research Projects Agency (DARPA) under contract no. HR001118C0036; German Academic Exchange Services (DAAD); First Solar; TotalEnergies; Eni S.p.A. through the MIT Energy Initiative; University of Toronto's Acceleration Consortium; and U.S. Department of Energy's Office of Energy Efficiency and Renewable Energy (EERE) under the Solar Energy Technology Office (SETO) Award Number DE-EE0010503. This work made use of the MRSEC Shared Experimental Facilities at MIT, supported by the National Science Foundation under award number DMR-1419807.

References

1 S. L. Moskowitz, *Advanced materials innovation: Managing global technology in the 21st century*, John Wiley & Sons, 2016.
2 C. L. Magee, *Complexity*, 2012, **18**, 10–25.
3 Z. Wang, Z. Sun, H. Yin, X. Liu, J. Wang, H. Zhao, C. H. Pang, T. Wu, S. Li, Z. Yin, *et al.*, *Adv. Mater.*, 2022, **34**, 2104113.
4 C. Rao, *J. Mater. Chem.*, 1999, **9**, 1–14.
5 J. J. Hanak, The "multiple-sample concept" in materials research: Synthesis, compositional analysis and testing of entire multicomponent systems, *J. Mater. Sci.*, 1970, **5**, 964–971.
6 B. P. MacLeod, F. G. Parlane, C. C. Rupnow, K. E. Dettelbach, M. S. Elliott, T. D. Morrissey, T. H. Haley, O. Proskurin, M. B. Rooney, N. Taherimakhsousi, *et al.*, *Nat. Commun.*, 2022, **13**, 995.
7 K. Hippalgaonkar, Q. Li, X. Wang, J. W. Fisher III, J. Kirkpatrick and T. Buonassisi, *Nat. Rev. Mater.*, 2023, **8**, 241–260.
8 T. Wang, R. Li, H. Ardekani, L. Serrano-Lujan, J. Wang, M. Ramezani, R. Wilmington, M. Chauhan, R. W. Epps, K. Darabi, *et al.*, *Matter*, 2023, **6**, 2963–2986.
9 A. E. Gongora, B. Xu, W. Perry, C. Okoye, P. Riley, K. G. Reyes, E. F. Morgan and K. A. Brown, *Sci. Adv.*, 2020, **6**, 1–6.
10 P. Liu, B. Guo, T. An, H. Fang, G. Zhu, C. Jiang and X. Jiang, *J. Materiomics*, 2017, **3**, 202–208.
11 I. Yanase, T. Ohtaki and M. Watanabe, *Solid State Ionics*, 2002, **151**, 189–196.
12 M. Zeng, Y. Du, Q. Jiang, N. Kempf, C. Wei, M. V. Bimrose, A. N. Tanvir, H. Xu, J. Chen, D. J. Kirsch, J. Martin, B. C. Wyatt, T. Hayashi, M. Saeidi-Javash, H. Sakaue, B. Anasori, L. Jin, M. D. McMurtrey and Y. Zhang, *Nature*, 2023, **617**(7960), 292–298.
13 D. Bash, Y. Cai, V. Chellappan, S. L. Wong, X. Yang, P. Kumar, J. D. Tan, A. Abutaha, J. J. Cheng, Y.-F. Lim, S. I. P. Tian, Z. Ren, F. Mekki-Berrada, W. K. Wong, J. Xie, J. Kumar, S. A. Khan, Q. Li, T. Buonassisi and K. Hippalgaonkar, *Adv. Funct. Mater.*, 2021, **31**, 2102606.
14 S. Langner, F. Häse, J. D. Perea, T. Stubhan, J. Hauch, L. M. Roch, T. Heumueller, A. Aspuru-Guzik and C. J. Brabec, *Adv. Mater.*, 2020, **32**, 1907801.

15 T. C. Wu, A. Aguilar-Granda, K. Hotta, S. A. Yazdani, R. Pollice, J. Vestfrid, H. Hao, C. Lavigne, M. Seifrid, N. Angello, *et al.*, *Adv. Mater.*, 2023, **35**, 2207070.
16 S. Lo, S. G. Baird, J. Schrier, B. Blaiszik, N. Carson, I. Foster, A. Aguilar-Granda, S. V. Kalinin, B. Maruyama, M. Politi, H. Tran, T. D. Sparks and A. Aspuru-Guzik, *Digital Discovery*, 2024, **3**, 842–868.
17 A. Pandian and C. Belavek, *2016 ASEE North Central Section Conference*, 2016.
18 G. R. Allen, *et al.*, *Record West Aust. Mus.*, 1978, **6**, 355–378.
19 A. E. Siemenn, *A System for High-Throughput Materials Exploration Driven by Machine Learning*, 2021.
20 A. E. Siemenn, E. Shaulsky, M. Beveridge, T. Buonassisi, S. M. Hashmi and I. Drori, *ACS Appl. Mater. Interfaces*, 2022, **14**, 4668–4679.
21 A. E. Siemenn, E. Aissi, F. Sheng, A. Tiihonen, H. Kavak, B. Das and T. Buonassisi, *Nat. Commun.*, 2024, **15**, 4654.
22 L. M. Ellram, *Int. J. Phys. Distrib. Logist. Manag.*, 1995, **25**, 4–23.
23 W. Ouyang, R. W. Bowman, H. Wang, K. E. Bumke, J. T. Collins, O. Spjuth, J. Carreras-Puigvert and B. Diederich, *Adv. Biol.*, 2022, **6**, 2101063.
24 K. Potgieter and R. Meijboom, *J. Chem. Technol. Biotechnol.*, 2021, **96**, 2547–2557.
25 L. Yang, J. A. Haber, Z. Armstrong, S. J. Yang, K. Kan, L. Zhou, M. H. Richter, C. Roat, N. Wagner, M. Coram, M. Berndl, P. Riley and J. M. Gregoire, *Proc. Natl. Acad. Sci. U. S. A.*, 2021, **118**, e2106042118.
26 A. D. Collord, H. Xin and H. W. Hillhouse, *IEEE J. Photovoltaics*, 2015, **5**, 288–298.
27 J. M. Gregoire, L. Zhou and J. A. Haber, *Nat. Synth.*, 2023, **2**, 493–504.
28 R. Potyrailo, K. Rajan, K. Stoewe, I. Takeuchi, B. Chisholm and H. Lam, *ACS Comb. Sci.*, 2011, **13**, 579–633.
29 M. Abolhasani and E. Kumacheva, *Nat. Synth.*, 2023, **2**, 483–492.
30 R. W. Epps, K. C. Felton, C. W. Coley and M. Abolhasani, *Lab Chip*, 2017, **17**, 4040–4047.
31 T. S. Kaminski and P. Garstecki, *Chem. Soc. Rev.*, 2017, **46**, 6210–6226.
32 A. Slattery, Z. Wen, P. Tenblad, J. Sanjosé-Orduna, D. Pintossi, T. den Hartog and T. Noël, *Science*, 2024, **383**, eadj1817.
33 A. Charalampidou, T. Nehls, C. Meyners, S. Gandhesiri, S. Pomplun, B. L. Pentelute, F. Lermyte and F. Hausch, *ACS Cent. Sci.*, 2024, **10**, 649–657.
34 J. Li, Y. Tu, R. Liu, Y. Lu and X. Zhu, *Adv. Sc.*, 2020, **7**, 1901957.
35 N. J. Szymanski, B. Rendy, Y. Fei, R. E. Kumar, T. He, D. Milsted, M. J. McDermott, M. Gallant, E. D. Cubuk, A. Merchant, H. Kim, A. Jain, C. J. Bartel, K. Persson, Y. Zeng and G. Ceder, *Nature*, 2023, **624**, 86–91.
36 S. B. Harris, A. Biswas, S. J. Yun, K. M. Roccapriore, C. M. Rouleau, A. A. Puretzky, R. K. Vasudevan, D. B. Geohegan and K. Xiao, *Small Methods*, 2024, 2301763.
37 J. Wagner, C. G. Berger, X. Du, T. Stubhan, J. A. Hauch and C. J. Brabec, *J. Mater. Sci.*, 2021, **56**, 16422–16446.
38 J. Zhang, J. A. Hauch and C. J. Brabec, *Acc. Chem. Res.*, 2024, **57**, 1434–1445.
39 P. Shiri, V. Lai, T. Zepel, D. Griffin, J. Reifman, S. Clark, S. Grunert, L. P. Yunker, S. Steiner, H. Situ, F. Yang, P. L. Prieto and J. E. Hein, *iScience*, 2021, **24**, 102176.
40 J. Schrier and A. J. Norquist, *Methods and Applications of Autonomous Experimentation*, Chapman and Hall/CRC, 2023.
41 J. Schrier, A. J. Norquist, T. Buonassisi and J. Brgoch, *J. Am. Chem. Soc.*, 2023, **145**, 21699–21716.
42 E. J. Kluender, J. L. Hedrick, K. A. Brown, R. Rao, B. Meckes, J. S. Du, L. M. Moreau, B. Maruyama and C. A. Mirkin, *Proc. Natl. Acad. Sci. U. S. A.*, 2019, **116**, 40–45.
43 D. Caramelli, D. Salley, A. Henson, G. A. Camarasa, S. Sharabi, G. Keenan and L. Cronin, *Nat. Commun.*, 2018, **9**, 3406.
44 M. A. Flores-Ortiz, R. A. Gutiérrez-Márquez, R. S. Mier-Jiménez, M. M. Flores-Leonar and A. Aguilar Granda, Building C-C bonds using a cheap automated synthesis platform, *ChemRxiv*, 2023, preprint, DOI: **10.26434/chemrxiv-2023-x0l8f**.
45 M. Politi, F. Baum, K. Vaddi, E. Antonio, J. Vasquez, B. P. Bishop, N. Peek, V. C. Holmberg and L. D. Pozzo, *Digital Discovery*, 2023, **2**, 1042–1057.
46 Y. Xie, C. Zhang, H. Deng, B. Zheng, J.-W. Su, K. Shutt and J. Lin, *ACS Appl. Mater. Interfaces*, 2021, **13**, 53485–53491.
47 M. A. Shah, D.-G. Lee, B.-Y. Lee and S. Hur, *IEEE Access*, 2021, **9**, 140079–140102.
48 X. Deng, H. Li and Y. Song, *Giant*, 2024, **17**, 100222.
49 D. Guevarra, A. Shinde, S. K. Suram, I. D. Sharp, F. M. Toma, J. A. Haber and J. M. Gregoire, *Energy Environ. Sci.*, 2016, **9**, 565–580.
50 F. Mathies, E. J. W. List-Kratochvil and E. L. Unger, *Energy Technol.*, 2020, **8**, 1900991.
51 S. Chen, L. Zhang, L. Yan, X. Xiang, X. Zhao, S. Yang and B. Xu, *Adv. Funct. Mater.*, 2019, **29**, 1905487.
52 Y. Cheng, H. Wu, J. Ma, P. Li, Z. Gu, S. Zang, L. Han, Y. Zhang and Y. Song, *CCS Chem.*, 2022, **4**, 1465–1485.
53 L. Yang, J. A. Haber, Z. Armstrong, S. J. Yang, K. Kan, L. Zhou, M. H. Richter, C. Roat, N. Wagner, M. Coram, *et al.*, *Proc. Natl. Acad. Sci. U. S. A.*, 2021, **118**, e2106042118.
54 L. Shi, L. Meng, F. Jiang, Y. Ge, F. Li, X.-g. Wu and H. Zhong, *Adv. Funct. Mater.*, 2019, **29**, 1903648.
55 I. D. Styliari, C. Conte, A. K. Pearce, A. Hüsler, R. J. Cavanagh, M. J. Limo, D. Gordhan, A. Nieto-Orellana, J. Suksiriworapong, B. Couturaud, P. Williams, A. L. Hook, M. R. Alexander, M. C. Garnett, C. Alexander, J. C. Burley and V. Taresco, *Macromol. Mater. Eng.*, 2018, **303**, 1800146.
56 A. Queraltó, J. Banchewski, A. Pacheco, K. Gupta, L. Saltarelli, D. Garcia, N. Alcalde, C. Mocuta, S. Ricart, F. Pino, X. Obradors and T. Puig, *ACS Appl. Mater. Interfaces*, 2021, **13**, 9101–9112.
57 A. L. Roy, H. N. Chiu and K. Walus, *Lab Chip*, 2021, **21**, 4427–4436.
58 S. E. Evans, T. Harrington, M. C. Rodriguez Rivero, E. Rognin, T. Tuladhar and R. Daly, *Int. J. Pharm.*, 2021, **599**, 120443.

59 I. D. Styliari, C. Conte, A. K. Pearce, A. Hüsler, R. J. Cavanagh, M. J. Limo, D. Gordhan, A. Nieto-Orellana, J. Suksiriworapong, B. Couturaud, *et al.*, *Macromol. Mater. Eng.*, 2018, **303**, 1800146.
60 C.-C. Huang, Z.-K. Kao and Y.-C. Liao, *ACS Appl. Mater. Interfaces*, 2013, **5**, 12954–12959.
61 D. Bernoulli, *Hydrodynamica, Apud Johannem Reinholdum Dulseckern*, 1738.
62 K. Ward and Z. H. Fan, *J. Micromech. Microeng.*, 2015, **25**, 1–15.
63 P. R. Fortes, M. A. Feres, M. K. Sasaki, E. R. Alves, E. A. Zagatto, J. A. Prior, J. L. Santos and J. L. Lima, *Talanta*, 2009, **79**, 978–983.
64 O. Reynolds, *Philos. Trans. R. Soc. London*, 1883, **174**, 935–982.
65 N. Ryan and M. Johnson, *AIChE J.*, 1959, **5**, 433–435.
66 S. A. Vagner, S. A. Patlazhan, C. A. Serra and D. Funfschilling, *Phys. Fluids*, 2021, **33**, 072010.
67 P. Lin, Q. Chen, Y. Liu, X. Hu and Z. Zhu, *ACS Omega*, 2022, **7**, 23890–23898.
68 K. Mutschler, S. Dwivedi, S. Kartmann, S. Bammesberger, P. Koltay, R. Zengerle and L. Tanguy, *Mechatronics*, 2014, **24**, 209–221.
69 M. B. Mbanjwa, K. Harding and I. M. Gledhill, *Micromachines*, 2022, **13**, 708.
70 A. Tiribocchi, A. Montessori, M. Lauricella, F. Bonaccorso, S. Succi, S. Aime, M. Milani and D. A. Weitz, *Nat. Commun.*, 2021, **12**(1), 1–10.
71 A. C. Brown and D. De Beer, *2013 Africon*, 2013, pp. 1–5.
72 R. Sliz, J. Czajkowski and T. Fabritius, *Langmuir*, 2020, **36**, 9562–9570.